

Two-zone Hugoniot for porous materials

A. D. Resnyansky*

WCSD, Defence Science and Technology Organisation, P.O. Box 1500, Edinburgh SA 5111, Australia

(Received 13 April 2015; revised manuscript received 3 November 2015; published 1 February 2016)

By decoupling thermal equilibrium conditions in shock loaded porous materials, two regimes resulting in two-zone Hugoniot are revealed, specifically, a stable low-pressure regime characterized by achieving interphase temperature equilibrium and a metastable high-pressure regime. Porous materials, represented as two-phase mixtures, are analyzed with an analytically constructed Hugoniot employing a constant Grüneisen parameter of condensed phase. Results of the analysis agree well with experiments for various porous materials over a wide range of porosities, which confirms the consistency of this interpretation. The two-zone consideration discovers a limitation on the high-temperature states of solid materials accessible via the shock loading of porous materials and suggests that the two-phase nature of porous materials needs to be reflected in the use of Hugoniot data of powders when constructing equations of state for the corresponding condensed materials.

DOI: [10.1103/PhysRevB.93.054103](https://doi.org/10.1103/PhysRevB.93.054103)**I. INTRODUCTION**

A description of the shock compression of materials requires reliable equations of state. The Mie-Grüneisen equation of state (EOS) with a Grüneisen parameter that is constant [1] or slightly variable with volume [2], describes a wide variety of condensed materials very well [1–3]. Therefore, failure of this EOS to describe similar behavior of porous materials at high porosities in the megabar pressure range is challenging. The shock compression of porous materials is accompanied by extreme heating, which is formally conjectured from the energy balance between the states adjacent to a presumptive single shock jump [4]. The excessive heating is assumed to be caused by highly localized deformation and damage of particles constituting the material and is frequently attributed to the condensed constituent. The extreme temperature is considered to be a dominant factor of the description failure [5], which is responsible for transfer of the solid phase to a dense plasma state [5,6] and even to a gaseous state [7]. To improve the description of the behavior of powders by the solid EOSs, the latter are usually corrected by electronic terms associated with the quantum-mechanical effects resulting in a Grüneisen parameter variable with temperature or pressure [5,6].

However, several points of the traditional approach may need to be scrutinized. First, the temperature obtained from the single-jump assumption is an upper bound estimate because the initial and final states associated with a shock wave in porous material are likely to be connected through several smaller jumps and ramped compression waves [8–13]. Secondly, the transition of a nonorganic solid to a dense plasma requires a several times initial density compression and several tens of thousands of degrees heating [14], which is hard to supply even within the upper bound estimate. At the same time, the megabar shock compression of solid materials is unlikely to cause the electronic effects as discussed in Ref. [15]. A negligible contribution of preheating to the Hugoniot behavior of a condensed material was also noted in Ref. [16]. In addition, microstructure examinations of recovered 50% porosity steel powder samples [17] subjected to the shock compression with

pressures up to several tens of GPa demonstrate just a surface melting of the grains. According to microstructure observations [17,18] and experimental evaluations of temperature at dynamic deformation [19] and fracture [20] of solid materials, the extreme temperatures in the condensed phase of a porous material followed by the transformation to gaseous products are unlikely for nonorganic powders although this might be possible for some polymer powders [7].

Thus, attribution of the excessive heat solely to the condensed constituent could be in question (see a rather complete list of possible factors affecting the shock compression of powders in Ref. [18]). Analytical assessments [21,22] and mesoscale modeling [23] have suggested that the extreme temperature can be accounted for by the influence of interstitial gas, from which energy contribution is small mechanically but could be considerable thermally. Earlier, attempts to consider transfer of the heat due to adiabatic compression of trapped air to the condensed phase were undertaken in Refs. [24]. Involvement of the gaseous phase raises the problem of interphase equilibrium. A possible effect of this factor is an evolution of thermodynamic states behind the shock front, which has been studied experimentally [25] and numerically [11]. A recent attempt was made to incorporate the kinetic evolution of the behind-shock state into an EOS of a porous material considered as a single-phase medium [26].

Porous material is a material with a complex structure. Experimental studies of dynamic response usually employ a high strain rate split Hopkinson pressure bar testing technique for the investigation of sensitivity of the material response to the effects of structure, particle shape, and connectivity [27–30]. However, the pressure range relevant to these effects does not exceed the strength of the condensed phase, which is related to “nonhydrodynamic” effects and out of the scope of the present work.

The real experiment on porous material involving the factors of material structure and experimental setup can be numerically analyzed with a continuum constitutive model [11], including the kinetic effects from material microstructure. Despite the apparent difficulty of identifying Hugoniot states in continuum considerations due to the state evolution behind the shock front, even at the microlevel the use of molecular modeling for analysis of fluctuations of thermodynamic

*anatoly.resnyansky@dsto.defence.gov.au

parameters in blocks of atoms with voids (pores) under the shock loading conditions has been known for several decades [31], and recently molecular modeling has been used for a similar analysis with gas filled pores [32]. Moreover, the nonequilibrium molecular dynamics (NEMD) modeling has been advanced with a construct, known as Hugoniotat, linking the states separated by a shock wave [33].

While NEMD [31–33], mesomechanical [21,23,34], and phenomenological [10–12,26,35] simulations can provide detailed information about bulk material response and internal processes, including the effects taken into account by microstructure parameters of models, the corresponding modeling tools require specific information about the test setup, which is not usually available from the Hugoniot data repositories. Therefore, a widely spread technique is still the Hugoniot analysis based on jump conditions derived from phenomenological material models.

The present Hugoniot relations are derived from an analysis of thermodynamic states when representing porous material as a two-phase mixture with an internal dissipation mechanism that is responsible for adequate description of available experiments. A similar technique has been used for the Hugoniot analysis of a condensed mixture [36].

References [11,37] discuss reaching the interphase pressure and velocity equilibrium behind the shock front in the “hydrodynamic” approximation, i.e., neglecting the particle prepacking in a wave associated with the acoustic precursor and ignoring the strength effects. While accepting this approximation in the present work, interphase temperature relaxation within the shock loading zone may take considerable time requiring sufficiently long thermal contact between gaseous and solid phases, which results in a condition referred to as the PTE (pressure and temperature equilibrium) state. The conditions of reaching the thermal equilibrium have been analyzed and discussed in Ref. [11]. At the microlevel, the importance of heat exchange between interstitial gas and condensed material during the shock compression has recently been demonstrated by molecular modeling [32].

The constitutive modeling [11] has revealed a pressure threshold separating the PTE stable state from a metastable Hugoniot state with interphase temperature nonequilibrium within the shock zone and referred to as the PE (pressure equilibrium) state. The analysis suggested that the metastable Hugoniot state taken by the porous material is realized at pressures higher than the threshold. The pressure threshold corresponds to an intersection point (referred to in the present paper as the PE-PTE point) of the metastable PE and stable PTE loci on the pressure-volume plane. An important conclusion from the simulation of shock wave profiles [10,38] and analysis of the state evolution behind the shock front [10,11] validated against experiment is that the profiles observed in the simulations of porous materials can be considered quasistationary for a duration comparable with the duration of the experimental traces recorded in the Hugoniot tests. Thus, despite the complexity of the material and the process, Hugoniot states can be identified and associated with corresponding experimental values.

The nonlinear modeling [11] can accurately describe the transition between PE and PTE states caused by load variations, however, this description is possible only via a numerical

analysis. At the same time, the nature of the transition is hard to reveal from simulations. The present analytical consideration accompanied by a mesomechanical analysis demonstrates that the transition from the anomalous behavior in the PTE zone to the conventional behavior in the PE zone is a representation of the transition from unrestrained expansion of the condensed phase for a highly porous material at a moderate loading below the PE-PTE point (when the corresponding temperature rise expands the solid phase on a volume smaller than the volume of the shock compressed air) to the confined expansion at pressure above the PE-PTE point (when the corresponding temperature is sufficiently high in order to expand the solid phase on the volume exceeding the air gap). Thus, this point corresponds to the state of collapse of pores in the material.

The present analysis addresses the physical nature of these two regimes in a general multiphase representation of porous material, substantially ignoring the specifics of the material. In summary, the present consideration enables us (i) to derive an analytical Hugoniot, (ii) to explicitly formulate the abnormality condition, (iii) to reveal a link between the Hugoniot of porous material with that of the corresponding condensed material, and (iv) to reveal the mechanism of transition between the PTE and PE Hugoniots.

II. THEORY

The classical Hugoniot analysis [4] assumes equilibrium states ahead of and behind a shock front moving with speed D . The Rankine-Hugoniot (RH) conditions can be formulated using the conservation laws for mass, $\rho(D - u) = \rho_s D$, momentum, $p - p_s = \rho_s D u$, and energy with the last expressed as

$$e - e_s - \frac{1}{2}(p + p_s)\left(\frac{1}{\rho_s} - \frac{1}{\rho}\right) = 0, \quad (1)$$

where parameters are in the coordinate system associated with a stationary state (referred to as “s”) in front of the shock wave. Here, e is specific internal energy, ρ is material density determining specific volume as $v = 1/\rho$, p is pressure, and u is particle velocity. Thus, Eq. (1) is sufficient for the derivation of the Hugoniot in the form $p = p_H(v)$ if an EOS is given as $e = e(p, v)$.

In contrast to the classical analysis that can be completed with the above EOS and applied to a single-phase material, the present analysis is dealing with a two-phase material. Loading of multiphase materials is complemented with internal thermodynamic fluxes that are responsible for extra dissipation in the materials [35,36]. Referring to the phenomenological models [11,35] for multiphase materials, typical internal dissipation mechanisms are the mass, momentum, and heat exchange between the phases that may take the role of the thermodynamic fluxes.

For the present case of a porous material we assume the absence of mass exchange between the gaseous and condensed phases. The pressure and velocity equilibrium assumptions result in the absence of interphase momentum exchange. Thus, we cannot neglect only the interphase heat exchange taken as the internal process in the present case. Based on the framework discussed in Sec. I, we can conduct the Hugoniot analysis in two ultimate regimes: (i) the heat exchange has fully completed and the phases are in temperature equilibrium,

which requires an analysis of temperatures in the phases; and (ii) there is no heat exchange between the phases. The former provides complete thermodynamic equilibrium, whereas the latter is the conventional mixture approximation that ignores temperature difference between the phases. In reality, there might be a marginal zone of incomplete heat exchange, which requires a constitutive modeling [11] with a heat exchange kinetic incorporated. It is interesting to note, that the zone spreads very moderately away from the point of instantaneous transition between the regimes as observed for a number of porous materials in Refs. [10,11]. Therefore, we simplify the present consideration to the case of the instantaneous transition. Depending on the regimes, two separate Hugoniot need to be derived and analyzed.

The first step in realization of the suggested approach is to analyze Hugoniot in the PTE state. Variables' subscripts "1" and "2" refer to the condensed and gaseous phases, respectively. For a two-phase material, the mass-weighted additivity rule is applicable to the thermodynamical variables of specific internal energy and specific volume: $e = c_1 e_1 + c_2 e_2$, $v = c_1 v_1 + c_2 v_2$, where c_1 and c_2 are the corresponding mass concentrations. For the gaseous phase, we take the simplest EOS consistent with adiabatic shock compression—an ideal gas EOS, while the condensed phase utilizes the simplest generalization of the above EOS—the stiffened gas EOS. In this case, the EOSs formulated in the form of $e(p, v)$, are bilinear on p and v , as follows:

$$e_1 = \frac{p_1 + \gamma_1 p_{00}}{\gamma_{1m} \rho_1}, \quad e_2 = \frac{p_2}{\gamma_{2m} \rho_2}. \quad (2)$$

Here, $\gamma_{km} = \gamma_k - 1$, $\gamma_{kp} = \gamma_k + 1$, ($k = 1, 2$), where γ_{km} are the Grüneisen parameters (γ_2 is the polytropic index of the gas, with denotation $\Gamma = \gamma_{1m}$ used concurrently for the condensed phase), p_{00} is the stiffening constant in the EOS of the condensed phase ($p_{00} = \rho_{s1} c_1^2 / \gamma_1$), and c_1 is the bulk speed of sound. Having preset values for p_s , ρ_{s1} , c_1 , heat capacity c_{v1} , and Γ , we can fully specify the EOS. It is well known that this EOS is thermally inconsistent if adjusting realistic values of the sound speed and Grüneisen parameter with reference temperature T_0 . Therefore, T_0 is excluded from the list of parameters required for the EOS specification, thus neglecting a possible mismatch at nearly atmospheric conditions. This inconsistency is not critical in the hydrodynamic approximation of the present paper, and it can be easily rectified by using a rather simple nonlinear EOS generalization employed, for example, in Refs. [10,11]. However, the nonlinearity of the generalization precludes the Hugoniot for a porous material from an analytical representation. The advantage of using the stiffened gas EOS is that an analytically derived Hugoniot would allow us to conduct a mesomechanical analysis of the interphase exchange.

The ideal gas EOS at the reference state relates p_s , ρ_{s2} , and T_0 to heat capacity c_{v2} , γ_2 , and sound velocity c_2 . The constant e_s in Eq. (1) is calibrated such that $e = e_s$ at atmospheric pressure $p = p_k = p_s = p_a$ and $\rho_k = \rho_{sk}$ ($k = 1, 2$). We further denote $v_s = c_1 v_{s1} + c_2 v_{s2}$, where $v_{s1} = 1/\rho_{s1}$, $v_{s2} = 1/\rho_{s2}$. Variables p and v are not natural for the potential e , therefore, EOSs (2) should be completed with equations for

temperature

$$T_1 = \frac{1}{c_{v1}} \frac{p_1 + p_{00}}{\gamma_{1m} \rho_1}, \quad T_2 = \frac{1}{c_{v2}} \frac{p_2}{\gamma_{2m} \rho_2}. \quad (3)$$

Five equations (1)–(3) and two additivity rules for e and v are complemented with three equilibrium conditions for bulk and phase pressures $p = p_1$, $p_1 = p_2$, and phase temperatures $T_1 = T_2$. Thus, we obtain a system of ten equations for 11 independent variables: e , p , v , e_1 , e_2 , p_1 , p_2 , v_1 , v_2 , T_1 , and T_2 . When the above system is resolved for pressure against specific volume v , a quadratic equation for the Hugoniot $p = p_H(v)$ is obtained which has two solutions at the positive discriminant. Rewritten as $v = v_H(p)$, this equation facilitates analysis without multivaluedness

$$v = \frac{[\frac{1}{2}(p + p_s)v_s + e_s](c_{vm}p + c_{v2m}p_{00})}{p(c_{vs}p + c_{vg}p_{00}) + \frac{1}{2}(p + p_s)(c_{vm}p + c_{v2m}p_{00})}. \quad (4)$$

Here, we denote $c_{vs} = c'_1 + c'_2$, $c_{vg} = c'_1 \gamma_1 + c'_2$, $c_{vm} = c'_1 \gamma_{1m} + c'_2 \gamma_{2m}$, $c_{v2m} = c'_2 \gamma_{2m}$, $c_{vsm} = c_{vs} + \frac{1}{2} c_{vm}$, and $c_{vgm} = c_{vg} + \frac{1}{2} c_{v2m}$, where $c'_k = c_k c_{vk}$ ($k = 1, 2$). Thus, relation (4) is the PTE Hugoniot, $v_H^{PTE}(p)$, with the abnormality occurring when $\partial v_H^{PTE} / \partial p > 0$. The abnormality condition will be analyzed in detail in the next section.

Meanwhile, the shock transition with independent temperatures in the phases results in the PE Hugoniot $v_H^{PE}(p)$. In this case, each phase is subject to independent shock compression characterized by the same final pressure behind the shock front. Applying RH conditions (1) to individual phases with EOSs (2) results in well-known Hugoniot for both condensed and gaseous phases. These two Hugoniot, the additivity rule for specific volume, v , and two equilibrium conditions for the bulk and phase pressures, result in five equations for six variables p , v , p_1 , p_2 , v_1 , and v_2 . The solution of these equations, representing $v_H^{PE}(p)$, is

$$v = c_1 v_{s1} \frac{\gamma_{1p}(p_{00} + p_s) + \gamma_{1m}(p + p_s)}{\gamma_{1p}(p + p_s) + \gamma_{1m}(p_{00} + p_s)} + c_2 v_{s2} \frac{\gamma_{2p} p_s + \gamma_{2m} p}{\gamma_{2p} p + \gamma_{2m} p_s}. \quad (5)$$

Accepting the rule of transition from the PTE to PE Hugoniot at the PE-PTE point, which will also be discussed in more detail in the subsequent section, we obtain a single composite Hugoniot denoted by $v_H^S(p)$: $v_H^S(p) = \min\{v_H^{PTE}(p), v_H^{PE}(p)\}$. Cases beyond the assumption of instantaneous PE-PTE transition are governed by the kinetic of interphase heat transfer and can only be analyzed for powders with specified microstructure by using a constitutive model, e.g., the model described in Ref. [11].

III. ANALYSIS

Numerical examples of the present paper utilize the full-length analytical representation of the PTE Hugoniot (4), referred to in this section as $v_H(p)$. Simultaneously, for a convenient analysis of the abnormality, we consider an approximation of (4), $v_H^0(p)$, at $p_s = 0$. It is straightforward to prove for a pressure p a few orders higher than p_s , that the difference between the solutions v determined via $v_H(p)$ and

“phases” characterized by PE and PTE Hugoniot. Following the analysis in Ref. [11], we consider Rayleigh lines for the PE Hugoniot (lines R) and PTE Hugoniot (lines r) originating from point O , corresponding to the initial volume $v = v_s$. At the same pressure below the collapse point (pressure level A in Fig. 1), the shock velocity D^{PE} (slope of the R_A line) for the PE Hugoniot is larger than velocity D^{PTE} (slope of the r_A line) for the PTE Hugoniot: $D^{PE} > D^{PTE}$. Exactly at the collapse point: $D^{PE} = D^{PTE}$ (lines R_P and r_P are coincident), and at pressure above this point (pressure level B): $D^{PE} < D^{PTE}$ (slopes of lines R_B and r_B , respectively, in Fig. 1). Because the PE state is reached first, a two-wave configuration with a PE wave followed by a PTE wave is stable [11]. At the collapse point the waves are indistinguishable by pressure and density ($R_P = r_P$). In contrast, at pressure above the collapse point, a two-wave configuration cannot be stable due to the precedence of the PE state. As a result, a single PE wave is realized followed by a PTE state which is separated from the head wave by a temperature relaxation zone [11]. Using the chemical kinetics analogy, the head wave is an “overdriven” one followed by an equilibrium (stable) state tending to the PTE Hugoniot. A similar wave configuration was observed earlier in phase transition modeling [40]. The limited nature of this thermodynamic analogy should be noted due to the metastable character of the PE “phase” considered in this comment.

To support the note commented in the preceding section on the kinetic nature of the PE-PTE transition, we recall that the PE-PTE point corresponds to the pore collapse. Assessments of the collapse duration available in the literature even without consideration of the gaseous phase span from 200 ns [41] to more than a microsecond [42], which supports this note. The present analytical consideration assumes the shock transition in the phases. In the case of a ramped loading, the thermodynamic path of the corresponding transition may deviate from the PE or PTE Hugoniot. Thus, the load history governed by the transition kinetics in the corresponding compression wave determines the actual path. In general, when compared with the shock loading, the heating of the gaseous phase in the case of ramped load is lower due to a closer association with the isentropic loading and, as a result, expansion of the solid constituent is smaller, which tends to some quasi-isentropic PTE transition that has no abnormalities at any porosity in contrast to the shock PTE transition. Pointing to the kinetic nature, premature transition of the Hugoniot states to the PE branch following pressure rise is likely when thermal relaxation is not complete within the shock zone due to the material microstructure (e.g., anomalously large particles). On the contrary, delay of the transition to the PE branch or permanent association with the PTE branch is likely when the condensed phase converts to a substance with dramatically different mechanical properties (e.g., gasification of the solid phase).

IV. EXAMPLES

The present section presents Hugoniot calculated for several nonorganic and organic powders and compares the corresponding Hugoniot with experiments taken from popular collections of Hugoniot data [43–45]. The material constants

TABLE I. EOS constants for solid constituents of analyzed porous materials and calculated abnormality bounds of the two-phase powders.

	ρ_{s1} (g/cm ³)	c_1 (km/s)	c_{v1} [J/(g K)]	Γ	ρ_b (g/cm ³)	m_b
Cu	8.93	3.94	0.45	1.99	4.45	2.0
Fe	7.84	4.63	0.415	2.2	4.1	1.91
Ta ₂ O ₅	8.2	2.1	0.324	0.9	2.54	3.22
(C ₈ H ₈) _n	1.05	2.04	1.3	2.03	0.36	2.9
(C ₂ F ₄) _n (I)	2.17	1.47	1.17	0.45		
(C ₂ F ₄) _n (II)	2.355	4.0	0.5	1.4		
SiO ₂ (I)	2.65	3.77	0.75	1.55		
SiO ₂ (II)	4.29	8.57	0.9	2.3		

required by EOSs (2) and (3) are commonly available. Specifically, constants for air, including ρ_{s2} and c_{v2} , completed with two required extra constants $c_2 = 0.34$ km/s and $\gamma_2 = 1.4$, are obtained from (2) and (3) for the gaseous phase by adjustment of the constants with room temperature $T_0 = 300$ °K and atmospheric pressure $p_s = p_a = 0.1$ MPa. For the solid constituent of a powder, four constants are needed in order to specify the corresponding EOS: ρ_{s1} , c_1 , and c_{v1} —which are well tabulated—and Γ , taken as the corresponding value for the solid material, unless otherwise specified. The proposed analytical consideration relies on a constant Γ , which is consistent with the thermodynamic relation [4] for the Grüneisen parameter assessed as the ratio of volumetric heat expansion α on isentropic bulk modulus over density on the constant-pressure specific heat capacity. For solids at the reference conditions, the thermodynamic estimate of the Grüneisen parameter is very close to $\Gamma = \alpha c_s^2 / c_v$. Table I summarizes these constants for the corresponding condensed phases of the powders illustrated below.

The Hugoniot $v_H^s(p)$ for copper and iron powders are shown in Figs. 2 and 3, where the figure caption indicates values of porosity, $m = \rho_{s1} / \rho_s$ with denotation $\rho_s = 1 / v_s$. The points referred to in the present figure captions are experimental data. Tantalum pentoxide, Ta₂O₅, is illustrated in Fig. 4 with calculated composite Hugoniot for the corresponding powders that have recently been studied in several works [26,46,47]. Hugoniot for a polymer powder,

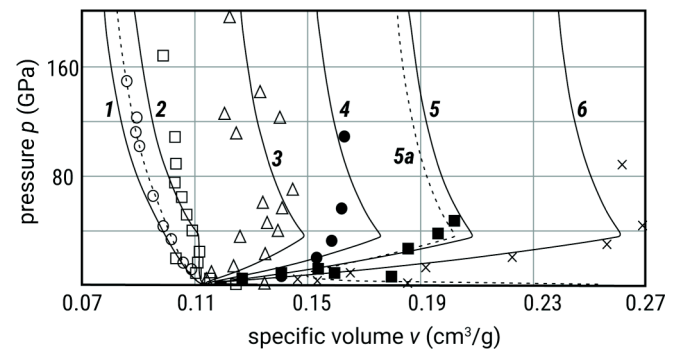


FIG. 2. Calculated composite Hugoniot (curves) compared to the experiment (points) for copper powders: $m = 1.4$ (1, \circ), 2 (2, \square), 4 (3, \triangle), 5.5 (4, \bullet), 7.2 (5, \blacksquare), and 10 (6, \times).

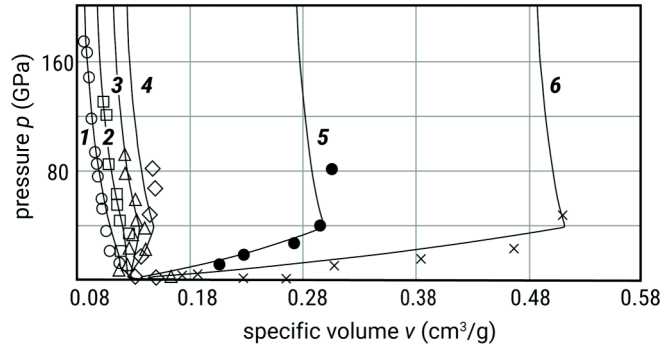


FIG. 3. Calculated composite Hugoniot (curves) compared to the experiment (points) for iron powders: $m = 1.13$ (1, \circ), 1.65 (2, \square), 2.33 (3, \triangle), 2.9 (4, \diamond), 10 (5, \bullet), and 20 (6, \times).

polystyrene (PS), $(C_8H_8)_n$, are shown in Fig. 5 and compared with experimental data from Refs. [44,45]. The anomalous behavior of polystyrene has previously been analyzed in Ref. [7] without explicit specification of individual experimental points.

The Grüneisen parameters of solid phases listed in Table I agree with the thermodynamic estimate for the majority of powders illustrated in Figs. 2–5. The Grüneisen parameter for the solid constituent of the tantalum pentoxide powder is taken as an average of the suggested values from Ref. [26].

Description of the experiments is generally good as seen in Figs. 2–5. The theory-experiment divergence at low porosities may reach nearly 8% for some powders with solid phases, such as copper, which exhibit a nonlinear cold compression response as shown in Fig. 2. Taking the nonlinearity into account in the Hugoniot calculation [11] for copper at $m = 1.4$ (dashed curve in Fig. 2 next to curve 1) proves that this divergence is due to the linear approximation of the present EOS.

At large porosities, the error magnitude of specific volume, Δv , due to experimental velocity errors ΔD and Δu can be assessed [5] from the RH conditions as a value proportional to the product of porosity, compression, and velocity errors. As a result, a 1% velocity error may cause the volume error to reach tens of percent for porosities higher than 5. To illustrate the error magnitude, evaluated error bars are shown for two experimental points from datasets in Figs. 4

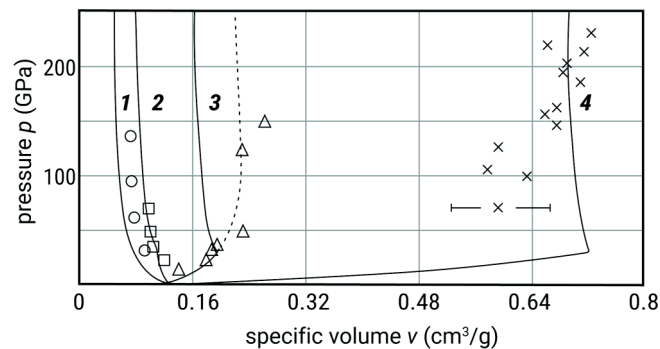


FIG. 4. Calculated composite Hugoniot (curves) compared to the experiment (points) for tantalum pentoxide powders: $m = 1.1$ (1, \circ), 2.7 (2, \square), 6.8 (3, \triangle), and 32.8 (4, \times).

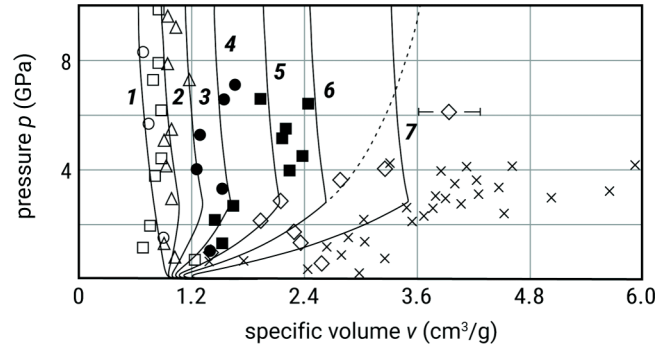


FIG. 5. Calculated composite Hugoniot (curves) compared to the experiment (points) for polystyrene powders: $m = 2.1$ (1, \circ), 3.67 (2, \square), 5.3 (3, \triangle), 7.2 (4, \bullet), 10.5 (5, \blacksquare), 13.6 (6, \diamond), and 19.1 (7, \times).

and 5. Accordingly, the theory and experiment in Figs. 2–5 for the high-porosity powders are in agreement within the experimental error margins.

Separately, two points above 100 GPa of the dataset 3 at $m = 6.8$ for the tantalum pentoxide powder (Fig. 4) were obtained in Z experiments [46], which provide conditions close to the isentropic compression [48]. The present consideration does not analyze an actual thermodynamic path for these loading conditions. Deviation of the two points from the composite Hugoniot (curve 3 in Fig. 4) is possibly associated with full dissociation of the gaseous phase to a monoatomic gas, which is caused by the joule heating to temperatures of at least a few up to several tens eV in the secondary hohlraums of Z-machine containing samples [49]. The dissociation may result in a variation [50] of the polytropic index in the gaseous phase (called isentropic coefficient in Ref. [50]) to $\gamma_2 = 5/3$. The result of the calculation employing this index for the gaseous phase (shown in Fig. 4 by a dashed curve) demonstrates that such a change in thermodynamic properties of the phase due to the specific loading conditions could be a reason for the deviation.

Meanwhile, the PTE Hugoniot offer a potentially better description of a polystyrene powder for points 6 and 7 in Fig. 5 (the dashed curve is the PTE Hugoniot for $m = 13.6$), scarcely available in the second Hugoniot zone. It should be noted that highly porous PS powders typically show a large experimental scatter (see comment on styrofoam in Ref. [3]). Possible proximity of the high-porosity experimental data to PTE Hugoniot could be caused by probable thermal decomposition [51] of polystyrene into gaseous products. The decomposition mechanism could be combustion because of the low limiting oxygen index (LOI) less than 20 [51]. The combustion results in more than 50% gaseous products [52] when oxygen is sufficiently supplied at high porosity. This mechanism has indirectly been confirmed by experiments [7] supported by a theory from the same paper, assuming transformation of the solid phase to a gaseous one. However, the datasets 6 and 7 do not provide a sufficiently wide range of points at high pressures above the collapse point, which makes it difficult to judge the validity of the combustion mechanism in this pressure region.

The suggested approach has been trialled on a wide range of powders with Hugoniot points from Refs. [43–45] when the high-porosity data were available. A comparison with experiments shows agreement of the description mostly within 10% when error margins are included. A description of similar adequacy was also observed for the materials where phase transition [such as the $(\alpha - \epsilon)$ transition in iron] does not result in a considerable change of mechanical impedance and Grüneisen parameter. Moreover, the predicted abnormality bounds, which are calculated using relation (6) and shown in Table I, agree particularly well with the values inferred from experimentally observed Hugoniots separating the normal and anomalous regimes (e.g., curve 2 in Fig. 2 as well as unshown separators at $m = m_b$ between curves 2 and 3 in Figs. 3 and 4, and between curves 1 and 2 in Fig. 5).

It is worthwhile comparing the “textbook” limiting porosity $m_t = (\Gamma + 2)/\Gamma$ with the limiting porosity m_b calculated from Eq. (6) and listed in Table I. It is seen that for the “heavy” powders with a large-density condensed phase the values of m_t and m_b are very close. However, the m_t assessment for a “light” powder with a low-density phase such as polystyrene, results in a value less than 2, whereas m_b is close to 3. At the same time, the experimental points for PS powder at $m = 2.1$ demonstrate that the dataset 1 in Fig. 5 does not show any abnormality. The anomalous behavior is observed for points 2 at $m = 3.67$, which agrees with the abnormality bound m_b . The reason for the divergence between m_b and m_t assessments is the omission of the second phase that becomes non-negligible in the calculation of m_b for the low-density condensed phase.

Thus, the present approach offers a good description and sensible interpretation that does not contradict available experiments. However, the case of phase transition may result in difficulties that cannot be resolved by the above two-phase approach and will be discussed in the next section.

V. MULTIPHASE GENERALIZATION

The phase transitions may result in a considerable impedance mismatch between polymorphs (such as those in silica powders), or in a substantial Γ variation (such as that in a Mie-Grüneisen EOS for polytetrafluoroethylene). In this case, the two-phase consideration of the previous sections is not applicable to the Hugoniot analysis for the corresponding porous materials. However, an analytical description is still possible for multiple phases in assumption of a constant phase composition during the shock loading.

The chosen assignment of phases assumes the first two phases to be polymorphic forms of the condensed phase related to each other by a transition from the first phase to the second one, and the third phase to be an interstitial gas. A simple generalization of the PTE Hugoniot from Sec. II for a three-phase material with two condensed phases and a third gaseous phase based on the same EOSs has the following form:

$$v = \frac{[\frac{1}{2}(p + p_s)v_s + e_s]A(p)}{\frac{1}{2}(p + p_s)A(p) + B(p)},$$

$$A(p) = c'_1\gamma_{1m}p_b p + c'_2\gamma_{2m}p_a p + c'_3\gamma_{3m}p_a p_b,$$

$$B(p) = c'_1p_b p_{ga} p + c'_2p_a p_{gb} p + c'_3p_a p_b p, \quad (8)$$

where $p_a = p + p_{01}$, $p_b = p + p_{02}$, $p_{ga} = p + \gamma_1 p_{01}$, and $p_{gb} = p + \gamma_2 p_{02}$, p_{0k} ($k = 1, 2$) are the stiffening constants of corresponding condensed phases, and denotations for the third gaseous phase are extended from the corresponding ones in Sec. II.

Similarly, an analytical representation of the PE Hugoniot is

$$v = c_1 v_{s1} \frac{\gamma_{1p}(p_{01} + p_s) + \gamma_{1m}(p + p_s)}{\gamma_{1p}(p + p_s) + \gamma_{1m}(p_{01} + p_s)} + c_2 v_{s2} \frac{\gamma_{2p}(p_{02} + p_s) + \gamma_{2m}(p + p_s)}{\gamma_{2p}(p + p_s) + \gamma_{2m}(p_{02} + p_s)} + c_3 v_{s3} \frac{\gamma_{3p} p_s + \gamma_{3m} p}{\gamma_{3p} p + \gamma_{3m} p_s}. \quad (9)$$

It should be noted that five formal combinations of PE and PTE states between the phases are possible. Hugoniots describing these combinations are also not difficult to derive in a similar way. However, for the sake of brevity, we consider only two of the above combinations out of the five: (i) all the phases are in thermal equilibrium [the Hugoniot v^{PTE} determined by Eq. (8)] and (ii) all the phases are in mutual thermal nonequilibrium [the Hugoniot v^{PE} determined by Eq. (9)].

To illustrate Hugoniots for the three-phase case, we analyze two porous materials with solid phases that are subject to phase transitions under shock loading, resulting in significantly different polymorphic modifications.

The first example considers polytetrafluoroethylene (PTFE), $(C_2F_4)_n$, powders. This material in condensed state has multiple phases, including a low-pressure crystalline phase that exhibits three forms at different temperatures mixed with an amorphous phase, all transforming to a high-pressure modification of the crystalline phase [53], when pressure is increasing. The physics of the phase transition is complex and requires a kinetic description embedded in the constitutive model such as that in Ref. [54].

A simplified approach in the present work employs a two-phase representation of the polymer, which is based on the fact that polymorphs of the low-pressure crystalline phase are mechanically relatively close to each other in comparison with the high-pressure crystalline phase. Thus, the simplified two-phase approximation of the material considers the first phase to be PTFE at normal conditions and the second phase to be the high-pressure crystalline phase. This approximation was used earlier for the two-phase modeling [55] of PTFE.

The high-pressure phase is not easy to characterize mechanically due to its metastable nature, but the modulus of this phase is expected to be relatively high as an analysis in Ref. [53] indicates. In addition, the isentrope data [56] suggest quite large sound speeds in solid PTFE under shock compression. The corresponding values for the second condensed phase of the represented material are shown in the “ c_1 ” column of Table I marked with the phase numbers referred to by roman numbers next to the chemical formula of the material. The Grüneisen parameter for the first condensed phase is taken from the thermodynamic estimate [56] and listed in Table I. However, when being under pressure, the Grüneisen parameter for PTFE is variable with both compression [56] and temperature [57]. The high compression value [56] of the

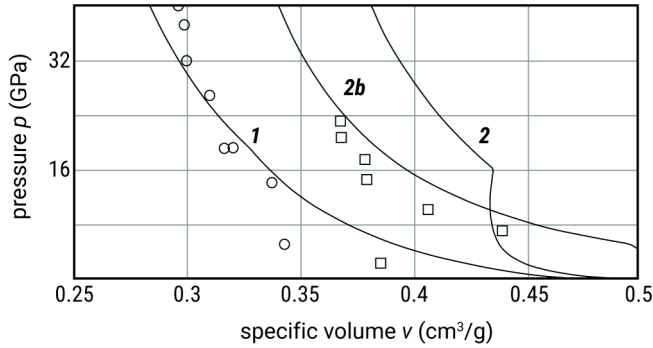


FIG. 6. Calculated three-phase composite Hugoniot (curves) compared to the experiment (points) for PTFE powders: $m = 1.45$ (1, \circ) and 2.82 (2, \square).

parameter selected for the second phase of PTFE is shown in Table I.

When increasing temperature, thermal decomposition is also a likely process as discussed in Ref. [56]. The influence of the decomposition or dissociation [56,58] on the mechanical properties, including the Grünesien parameter, is not easy to specify. In the case of limited air supply, possibly occurring in low-porosity powders and being observed in the recovery tests of solid PTFE [56], dissociation is more likely. In contrast, high-porosity powders can provide a high intake of oxygen at high pressure and temperature; therefore, the combustion is a possible mechanism of decomposition, even for a high LOI of PTFE [51] at normal conditions.

Calculated Hugoniot for PTFE are shown in Fig. 6 for relatively low (curve 1) and high (curve 2) porosities. At shock loading in the hydrodynamic pressure range, the transition of PTFE to the high-pressure zigzag conformation is accepted [53,54,56]. Therefore, the mass ratio of the second phase to the first, $c_2 : c_1$, which is needed for calculation of the phases' mass concentrations along with the given porosity $m = \rho_{s1}/\rho_s$, is taken to be 10:1. It is seen that the Hugoniot description is reasonable for the low-porosity case, but it is poor at high porosity. Possible disagreement could be associated with thermal decomposition, which could result in a drop of the Grünesien parameter (an example of a better description is demonstrated by curve 2b in Fig. 6 at $\Gamma_2 = 0.6$).

Another porous material illustrated in the present section is silicon dioxide (silica) undergoing a high-pressure transition to a metastable polymorphic form, stishovite [26]. The corresponding calculated Hugoniot are calculated and compared with experiments in Fig. 7.

Similarly to the preceding case, several low-pressure polymorphs exist in silica. In order to minimize the number of phases involved in the present analysis, we apply similar simplification as we used for PTFE. We choose the first phase at low pressure as α -quartz (for the crystalline silica) without distinguishing between low-pressure polymorphic modifications. The second phase at high pressure is taken to be stishovite [13]. It should be noted that this simplification is less rationalized for the present case within the hydrodynamic approximation because an intermediate phase, coesite, ignored in the present consideration, exists in a lower part of the hydrodynamic pressure range and its mechanical

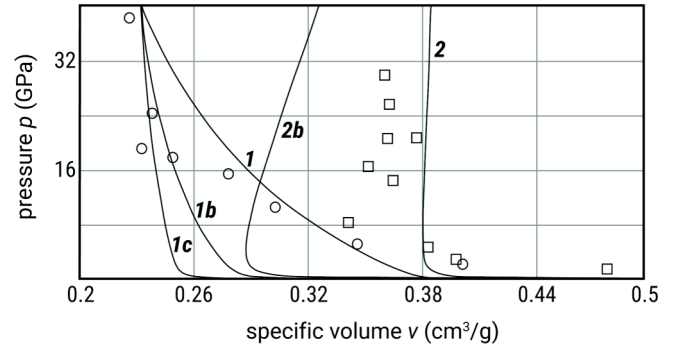


FIG. 7. Calculated three-phase composite Hugoniot (curves) compared to the experiment (points) for silicon dioxide powders: $m = 1.5$ (1, \circ) and 4.82 (2, \square).

characteristics differ notably from α -quartz and stishovite. The occurrence of this form begins at a relatively low pressure of nearly 2–3 GPa. We use α -quartz as the first phase because the coesite mechanical characteristics are closer to α -quartz than to stishovite, although an analysis with coesite as the first phase is equally possible. The mechanical characteristics and the Grünesien parameter for α -quartz and stishovite are taken from Refs. [59] and [60], respectively, and listed in Table I.

In both PTFE and silica, intermediate polymorphs may exist at a time when moving up along Hugoniot, resulting in a very complex process as molecular modeling [61] shows. Thus, these materials under shock compression do not preserve a permanent phase content, which is presumed by the present analysis. In order to associate the phase content with available experimental data for silica, we also choose several phase ratios, $c_2 : c_1$, within the condensed component of silica powders. For a moderate-porosity case at $m = 1.5$, curves 1, 1b, and 1c at the ratios 1:100, 3:1, and 10:1, respectively, demonstrate the influence of the phase content on the Hugoniot. It should be noted that while the phase transition develops in the shock zone, the Hugoniot in real powder may not follow the frozen Hugoniot shown in Fig. 7 because the Hugoniot, originating from points on Hugoniot with variable phase concentrations, take individual paths that may not be associated with any of the frozen Hugoniot.

As seen in Fig. 7, the calculated Hugoniot for the low-porosity powder describes experiments well in the low-pressure region, if the low-pressure phase is dominating (curve 1 at $c_2 : c_1 = 1 : 100$), whereas the description is poor in the high-pressure region. When increasing pressure, the description is improving with an increase of the stishovite concentration in the condensed component (curves 1b and 1c). For the high-porosity case, curves 2 and 2b correspond to the phase ratios 1:100 and 3:1, and the experimental points are in the region between these Hugoniot with prevailing low-pressure phase (curve 2) and high-pressure phase (curve 2a). This agrees with the widespread hypothesis of the presence of several polymorphs in silica during shock loading [13,59,60].

When comparing the low- and high-porosity cases of silica with experiments in Fig. 7 and keeping in mind the prevailing PTE regime for the high-porosity powder, the description of the shock compression of stishovite at low concentration is better for the high-porosity powder than for the low-porosity

powder. Therefore, one could conclude that expansion of the condensed phase as evidenced by the dominating PTE regime in the high-porosity case, limits concentration of stishovite in the condensed phase. Therefore, the volume change could be hypothesized to be a dominant kinetic driver of the phase transition in silica.

VI. INFLUENCE OF INTERSTITIAL GAS

The gaseous phase was frequently discarded from consideration in the shock compression analyses of porous materials available in the literature due to its low mechanical response when compared with the condensed phase. Several studies [5,62,63] have attempted to support the claim of negligible influence of the air phase by testing porous samples with evacuated air.

Referring to the experiments reported in Ref. [62], copper powder samples with the air evacuated down to a few Torr pressure (an order of several hundred Pa) have been tested under shock loading. However, this level of evacuation is not sufficient to achieve a sufficiently large free mean path [64] in order to assume the interstitial space being free of the air. Calculation of the composite Hugoniot using the relations from Sec. II, as well as numerical results [11] published earlier, give practically identical Hugoniots for powders under an initial pressure of 0.1 MPa and 500 Pa. It is interesting to note that the effect of initial air pressure in porous samples is more noticeable when calculating the shock compression of the corresponding samples with the elevated pressure of the interstitial air. For example, the calculation result of the composite Hugoniot for porous copper with initial air pressure of 10 MPa in the powder is shown as curve 5a in Fig. 2. However, lowering the pressure of the interstitial air down to tens of Pa as claimed in Refs. [5,63] results in large Knudsen numbers in the interstitial medium and a continuous analysis is not straightforwardly applicable, which requires an additional analysis.

First, we draw attention to the test methodology used for obtaining Hugoniot points. One of the most popular experimental techniques is the impedance match method outlined in Chapter 2 of Ref. [5]. The method is typically based on the time of arrival gauges (pins) which aim at recording the shock velocity in a material in parallel with measurement of the shock velocity for the same wave transmitted through a screen material (a standard). Numerical analysis of possible issues concerning the Hugoniot points of a porous material obtained with this technique has been conducted in Ref. [11]. However, evacuation of air from a porous sample raises additional issues to the Hugoniot interpretation, which will be addressed below.

Suppose that the air can be fully evacuated from a preselected original volume $A \times H$ that contains a certain mass of particles or a solid matrix occupying a volume $A \times h$ in a fully compacted state. Here, H and h are thicknesses of a porous and corresponding solid sample. Focusing on the shock wave propagation direction that is through the thickness direction, we can exclude the area dimension A .

First, we can calculate the shock wave propagation time, t_p , in a porous material sample occupying the original volume that consists of a solid matrix and the interstitial air at atmospheric conditions. Secondly, we assume that the air is fully evacuated

from the original volume of thickness H measured in the wave propagation direction.

When using time of arrival (TOA) gauges (e.g., pin gauges), the wave speed is calculated by division of the distance H over the propagation time t_v of a recordable shock disturbance. In accepting the mesomodel [21,65] simplification, it is easy to see that the propagation time t_v is a sum of propagation times through the condensed portion of the sample, t_c , and the time of movement of the screen transmitting shock wave to the sample, t_s . The solid portion of the sample could be a single block or an incremented set of matrix elements (e.g., particles), forming the same block after having removed voids. In turn, movement of the screen can either be broken down to a set of nonobstructed free movements of the particles through the empty space between the incremented set of particles or a continuous movement through the empty space of thickness $H - h$. In either case, the time contribution due to the propagation of disturbance through empty space spans over the same time, t_s .

Summarizing, in the case of evacuated air the resulting propagation time through the volume originally occupied by the sample is $t_v = t_c + t_s$. If the particle velocity behind the shock wave in the screen material due to impact by a flyer plate or acceleration by detonation products is U_p , then the free surface velocity (velocity of the screen surface moving towards the sample) is $2U_p$. Thus, $t_s = (H - h)/(2U_p)$ and $t_c = h/D_c$, where D_c is the shock wave velocity in the condensed phase.

The case with evacuated air, analyzed in Refs. [5,63], deals with two experimental Hugoniot points for silica powder. These points are among the experimental data considered for silica in the preceding section (Fig. 7). The samples were loaded by the shock wave corresponding to the velocity in an aluminum standard $U_p = 2.7$ km/s [63]. We consider times of arrival normalized by thickness H , which are in inverse velocity units, thus eliminating set-up dimensions from the analysis. Referring to the previous analysis, we consider the PTE and PE cases, where in the case of vacuum the interphase equilibrium relates only to the polymorphic modifications of the solid component of the powder.

We compare the normalized TOA for the porous material at the atmosphere conditions, t_p/H , with the TOA assessment $t_v/H = (t_s + t_c)/H$ calculated for the same assembly with evacuated air. The ratio $h/H \approx 1/m$ is calculated from known porosity m . The impedance match method with predetermined Hugoniot in the aluminum standard [5] allows us to calculate the Hugoniot state in the silica samples by employing the analytical Hugoniots of the preceding section. The results are summarized in Table II. In this table, $\rho_s = 0.55$ g/cm³ for the high-porosity case at $m = 4.82$ and $\rho_s = 1.75$ g/cm³ for the low-porosity case at $m = 1.5$. Pressure p_p is calculated in the powder at atmospheric conditions and p_c in the solid phase at the “vacuum” conditions. Indices S_p and S_c point to the interphase equilibrium conditions in the corresponding setups (the index S_p involves all three phases and the index S_c two condensed polymorphs).

It is seen from a comparison of t_p/H with t_v/H at the variety of interphase equilibrium conditions and several concentrations of the low- and high-pressure phases that the times differ from each other by a discrepancy from less than a percent up to 15%. Thus, the times of arrival do not differ

TABLE II. TOA evaluations in silica.

ρ_s (g/cm ³)	P_p (GPa)	P_c (GPa)	S_p	S_c	t_p/H (s/km)	t_v/H (s/km)	$c_1:c_2$
0.55	15.0	53.4	PTE	PTE	0.168	0.161	0.01
0.55	15.9	53.4	PE	PTE	0.157	0.161	0.01
0.55	15.8	68.4	PE	PTE	0.159	0.137	1.0
0.55	15.0	53.3	PTE	PE	0.168	0.162	0.01
0.55	15.9	53.3	PE	PE	0.157	0.162	0.01
0.55	15.8	65.1	PE	PE	0.159	0.146	1.0
1.75	40.5	77.7	PTE	PTE	0.153	0.147	3.0
1.75	40.5	77.7	PE	PTE	0.154	0.147	3.0
1.75	40.5	74.8	PTE	PE	0.153	0.152	3.0
1.75	40.5	74.8	PE	PE	0.153	0.152	3.0

dramatically for the atmospheric and vacuum conditions if the pin or similar TOA technique is used for registering the shock wave velocities, which means that the TOA proximity does not cast light on the influence of interstitial air on the Hugoniot.

It should be noted that evolution of the phase concentrations and conditions of equilibrium are kinetically driven, therefore, the present results are only possible estimates. However, the calculated TOA proximity is sufficient for the conclusion about the possible proximity of the shock velocities in powders filled up with vacuum and with the air at atmospheric conditions. Therefore, the Hugoniot states evaluated from the shock velocities using the RH relations in the vacuum setup may result in the pressure-volume response distant from that of the material. This is seen from p_s values in Table II, whereas the corresponding specific volume is hard to determine correctly in the vacuum setup due to the degenerating mass of the corresponding phase.

Thus, the pin technique cannot discriminate with certainty the shock compression of porous material at atmospheric conditions from that at the vacuum conditions only on the basis of TOA comparison. Embedded gauges [66] used for the shock testing of porous materials with explicit stress measurement or testing under elevated pressure could possibly bring more clarity to the issue of the air influence.

VII. DISCUSSION AND CONCLUSIONS

A Hugoniot relation in an analytical form has been derived, using the simplest EOSs for solid and gaseous phases of a porous material represented as a two-phase mixture. With the help of the analytical approach, a mesomechanical analysis of shock compression of the porous material has been conducted and two zones of Hugoniot have been revealed. The first stable zone is a result of full thermal expansion of the solid phase, when the limiting volume of the shock compressed gaseous phase is sufficiently large. The second zone corresponds to partial thermal expansion of the solid phase limited by the volume occupied by the shock compressed gaseous phase. Compression of the solid phase occurs as further expansion is attempted and is restricted by the limiting volume of the gaseous phase. The second zone is metastable with the material expanding further in a temperature relaxation zone.

A number of simplifications were used in the paper. For example, the shock compression of the phases of porous

material is represented on the mesolevel by equivalent elementary bulk compressions, which is quite different from the processes in real porous materials. The factors omitted in the present consideration are the three-dimensional nature of the compression on the mesolevel depending on the material microstructure, high-temperature variation of the polytropic index in the gaseous phase at shock compression, etc. The description of available experiments with the present approach, accepting these simplifications, is surprisingly good and indicates that the bulk compressive response of the powders in the hydrodynamic pressure region seemingly dominates.

Using the present analysis, the change of Hugoniot behavior from normal to anomalous regime when porosity is increasing could be explained by introducing a larger volume of the interstitial gas, which results in a larger heating of the shock compressed gaseous phase causing a larger thermal expansion of the solid phase that is expanded fully in the first Hugoniot zone. The abnormality condition obtained with the present approach below the collapse point is very close to the well-known abnormality limit in the case of heavy powders but may differ essentially for light powders and the condition cannot be applied above the collapse point.

Addressing thermodynamical aspects of the present analysis within the hydrodynamic and linear EOS approximations, pressure and temperature from the Hugoniot of a porous material in the first zone could be used for characterization of the condensed phase with specific volume apportioned to the first phase from the first equation of (7). Similar decomposition can be applied to the condensed phase in the second zone taking pressure, properly apportioned volume of the Hugoniot of the corresponding porous material (5), and temperature from the first equation of (3). Note, a state from the second metastable Hugoniot zone for the condensed phase does not necessarily correlate with the point of its phase diagram corresponding to the bulk temperature, evaluated from the energy balance for the porous material.

The present approach enables us to analyze the Hugoniot of multiphase porous materials. An analysis of porous materials with phase transition between two phases of solid constituents confirms an adequate correlation of the Hugoniots at various concentrations of the phase modifications with the pressure range corresponding to the prevailing phase modification. However, in addition to the requirement of an invariable Güneisen parameter of the condensed phase, the limitation of the analytical approach is a permanent phase composition which can be pulled off only by constitutive modeling with a phase transition kinetic.

Further more explicit experimental studies are necessary for clarification of the influence of the interstitial air on the Hugoniot behavior because the traditional impedance match technique cannot lead to an unambiguous conclusion. From the analysis, the porous material with evacuated air is seemingly thermodynamically different from porous material with an interstitial gas.

Summarizing, (1) the Hugoniot data for porous materials provide relevant data in thermodynamical equilibrium for the condensed phase in the first stable zone; (2) decomposition of the Hugoniot data for condensed materials from the Hugoniot data for porous materials has to be mediated by an analysis that takes into account the heat transfer from the gaseous

to the condensed phase. Specifically, the second metastable zone does not provide a thermodynamic equilibrium state, but can be used for generation of the required data via a two-phase consideration. A flowchart for determination of the data can be deduced from the analytical derivation in Sec. II; and (3) the thermodynamical properties, in particular, the Grüneisen parameter, available for condensed materials could possibly be applicable in areas of the phase diagram

of compliant porous materials with essentially higher thermal energy than was believed earlier, if the gaseous phase is taken into consideration. On the other hand, when temperatures are assessed from the energy balance at shock compression of porous materials, the extreme temperature data assigned to condensed materials in corresponding phase diagrams may not actually be achieved due to the temperature nonequilibrium in the second metastable Hugoniot zone.

-
- [1] R. G. McQueen and S. P. Marsh, *J. Appl. Phys.* **31**, 1253 (1960).
- [2] J. M. Walsh, M. H. Rice, R. G. McQueen, and F. L. Yarger, *Phys. Rev.* **108**, 196 (1957).
- [3] R. G. McQueen, S. P. Marsh, J. W. Taylor, and J. N. Fritz, in *High-Velocity Impact Phenomena*, edited by R. Kinslow (Academic, New York, 1970), pp. 293–417.
- [4] Ya. B. Zeldovich and Yu. P. Raiser, *Physics of Shock Waves and High Temperature Hydrodynamic Phenomena* (Academic, New York, 1967).
- [5] R. F. Trunin, *Shock Compression of Condensed Materials* (Cambridge University Press, Cambridge, UK, 1998).
- [6] L. Boshoff-Mostert and H. J. Viljoen, *J. Appl. Phys.* **86**, 1245 (1999).
- [7] L. G. Bolkhovitinov and Yu. B. Khvostov, *Nature (London)* **274**, 882 (1978).
- [8] J. M. Powers, D. S. Stewart, and H. Krier, *J. Appl. Mech.* **56**, 15 (1989).
- [9] D. P. Dandekar and R. M. Lamothe, *J. Appl. Phys.* **48**, 2871 (1977).
- [10] A. D. Resnyansky and N. K. Bourne, *J. Appl. Phys.* **95**, 1760 (2004); A. D. Resnyansky, *ibid.* **108**, 083534 (2010).
- [11] A. D. Resnyansky, *J. Appl. Phys.* **104**, 093511 (2008).
- [12] D. Grady, G. Fenton, and T. Vogler, *Int. J. Impact Eng.* **56**, 19 (2013).
- [13] D. E. Grady, W. J. Murri, and G. R. Fowles, *J. Geophys. Res.* **79**, 332 (1974).
- [14] S. Mazevet and G. Z erah, *Phys. Rev. Lett.* **101**, 155001 (2008).
- [15] W. J. Nellis, J. A. Moriarty, A. C. Mitchell, M. Ross, R. G. Dandrea, N. W. Ashcroft, N. C. Holmes, and G. R. Gathers, *Phys. Rev. Lett.* **60**, 1414 (1988).
- [16] T. Sekine and T. J. Ahrens, in *Shock Compression of Condensed Matter 1991*, edited by S. C. Schmidt, R. D. Dick, J. W. Forbes, D. G. Tasker (Elsevier, Amsterdam, 1992), pp. 57–60.
- [17] W. H. Gourdin, *J. Appl. Phys.* **55**, 172 (1984); J. E. Flinn, R. L. Williamson, R. A. Berry, R. N. Wright, Y. M. Gupta, and M. Williams, *ibid.* **64**, 1446 (1988).
- [18] S. S. Shang, D. J. Benson, and M. A. Meyers, *J. Phys. IV* **4**, C8-521 (1994).
- [19] J. Duffy, in *Mechanics of Material Behavior*, edited by G. Dvorak and R. T. Shield (Elsevier, Amsterdam, 1984), pp. 75–86.
- [20] A. J. Rosakis, J. J. Mason, and G. Ravichandran, *J. Mech. Behav. Mater.* **4**, 375 (1993).
- [21] V. F. Lotrich, T. Akashi, and A. B. Sawaoka, in *Metallurgical Applications of Shock-Wave and High-Strain Rate Phenomena*, edited by L. E. Murr, K. P. Staudhammer, and M. A. Meyers (Marcel Dekker, New York, 1986), Chap. 13, pp. 277–292.
- [22] T. Kobayashi, *Chem. Phys. Lett.* **565**, 35 (2013).
- [23] R. L. Williamson, *J. Appl. Phys.* **68**, 1287 (1998).
- [24] I. M. Voskoboinikov, A. N. Afanasev, and V. M. Bogomolov, *Combust. Explos. Shock Waves* **3**, 359 (1967); V. S. Trofimov, *ibid.* **3**, 352 (1967); Yu. L. Alekseev, V. P. Ratnikov, and A. P. Rybakov, *J. Appl. Mech. Tech. Phys.* **12**, 257 (1971).
- [25] V. S. Trofimov, G. A. Adadurov, S. V. Pershin, and A. N. Dremin, *Combust., Explos. Shock Waves (Engl. Transl.)* **4**, 142 (1968).
- [26] G. Fenton, D. Grady, and T. J. Vogler, *Procedia Eng.* **58**, 724 (2013).
- [27] B. E. Martin, W. Chen, B. Song, and S. A. Akers, *Mech. Mater.* **41**, 786 (2009).
- [28] N. D. Parab, B. Claus, M. C. Hudspeth, J. T. Black, A. Mondal, J. Sun, K. Fezzaa, X. Xiao, S. N. Luo, and W. Chen, *Int. J. Impact Eng.* **68**, 8 (2014).
- [29] M. E. Kabir, B. Song, B. E. Martin, and W. Chen, Sandia National Laboratories Report No. SAND2010-2289, 2010.
- [30] M. Peroni, L. Peroni, and M. Avalle, *J. Phys. IV* **134**, 609 (2006).
- [31] J. W. Mintmire, D. H. Robertson, and C. T. White, *Phys. Rev. B* **49**, 14859 (1994).
- [32] L. Soulard, N. Pineau, J. Cl erouin, and L. Colombet, *J. Appl. Phys.* **117**, 115901 (2015).
- [33] J.-B. Maill et, M. Mareschal, L. Soulard, R. Ravelo, P. S. Lomdahl, T. C. Germann, and B. L. Holian, *Phys. Rev. E* **63**, 016121 (2000).
- [34] D. J. Benson, V. F. Nesterenko, F. Jonsdottir, and M. A. Meyers, *J. Mech. Phys. Solids* **45**, 1955 (1997).
- [35] R. I. Nigmatulin, *Dynamic of Multiphase Media* (Hemisphere, New York, 1990).
- [36] G. E. Duvall and S. M. Taylor, Jr., *J. Compos. Mater.* **5**, 130 (1971).
- [37] B. R. Krueger and T. Vreeland, Jr., *J. Appl. Phys.* **69**, 710 (1991).
- [38] A. D. Resnyansky and N. K. Bourne, *AIP Conf. Proc.* **706**, 1474 (2004).
- [39] W. J. Carter and S. P. Marsh, Los Alamos National Laboratory Report No. LA-UR-77-2062, 1977.
- [40] J. M. Winey and Y. M. Gupta, *Phys. Rev. B* **87**, 174104 (2013).
- [41] M. M. Carroll and A. C. Holt, *J. Appl. Phys.* **43**, 1626 (1972).
- [42] M. M. Carroll, K. T. Kim, and V. F. Nesterenko, *J. Appl. Phys.* **59**, 1962 (1986).
- [43] Compendium of Shock Wave Data, edited by M. van Thiel, Livermore National Laboratory Report No. UCRL-50108, 1977.
- [44] R. F. Trunin, L. F. Gudarenko, M. V. Zhernokletov, and G. V. Simakov, *Experimental Data on Shock Compression and*

- Adiabatic Expansion of Condensed Matter*, 2nd ed. (RFNC-VNIIEF, Sarov, Russia, 2006).
- [45] *LASL Shock Hugoniot Data*, edited by S. P. Marsh (University of California Press, Berkeley, 1980).
- [46] T. J. Vogler, S. Root, M. D. Knudson, and W. D. Reinhart, Sandia National Laboratories Report No. SAND2011-6770, 2011.
- [47] J. E. Miller, T. R. Boehly, D. D. Meyerhofer, and J. H. Eggert, *AIP Conf. Proc.* **955**, 71 (2007).
- [48] C. A. Hall, J. R. Asay, M. D. Knudson, W. A. Stygar, R. B. Spielman, T. D. Pointon, D. B. Reisman, A. Toor, and R. C. Cauble, *Rev. Sci. Instrum.* **72**, 3587 (2001).
- [49] T. Trucano, K. G. Budge, R. J. Lawrence, J. R. Asay, C. A. Hall, K. G. Holland, C. H. Konrad, W. D. Trott, G. A. Chandler, and K. Flemming, Sandia National Laboratories Report No. SAND99-1255, 1999.
- [50] M. Capitelli, G. Colonna, and A. D'Angola, *Fundamental Aspects of Plasma Chemical Physics: Thermodynamics* (Springer-Verlag, New York, 2012).
- [51] C. L. Beyler and M. M. Hirschler, in *SFPE Handbook of Fire Protection Engineering 2*, 3rd ed. (National Fire Protection Association, Quincy, MA, 2002), Sec. 1, Chap. 7, pp. 110–131.
- [52] R. A. Hawley-Fedder, M. L. Parsons, and F. W. Karasek, *J. Chromatogr., A* **315**, 201 (1984).
- [53] E. N. Brown, P. J. Rae, D. M. Dattelbaum, B. Clausen, and D. W. Brown, *Exp. Mech.* **48**, 119 (2008).
- [54] A. D. Resnyansky, N. K. Bourne, J. C. F. Millett, and E. N. Brown, *J. Appl. Phys.* **110**, 033530 (2011).
- [55] A. D. Resnyansky, N. K. Bourne, E. N. Brown, J. C. F. Millett, P. J. Rae, S. A. McDonald, and P. J. Withers, *J. Appl. Phys.* **116**, 223502 (2014).
- [56] C. E. Morris, J. N. Fritz, and R. G. McQueen, *J. Chem. Phys.* **80**, 5203 (1984).
- [57] S. R. Urzendowski, A. H. Guenther, and J. R. Asay, in *Analytical Calorimetry*, edited by R. S. Porter and J. F. Johnson (Plenum, New York, 1968), pp. 119–132.
- [58] A. N. García, N. Viciano, and R. Font, *J. Anal. Appl. Pyrolysis* **80**, 85 (2007).
- [59] H. Tan and T. J. Ahrens, *J. Appl. Phys.* **67**, 217 (1990).
- [60] J. A. Akins and T. J. Ahrens, *Geophys. Res. Lett.* **29**, 31-1 (2002).
- [61] J. M. D. Lane, A. P. Thompson, and T. J. Vogler, *Phys. Rev. B* **90**, 134311 (2014).
- [62] R. F. Trunin, G. V. Simakov, Yu. N. Sutulov, A. B. Medvedev, B. D. Rogozkin, and Yu. E. Fedorov, *Zh. Eksp. Teor. Fiz.* **96**, 1024 (1989) [*Sov. Phys. JETP* **69**, 580 (1989)].
- [63] G. V. Simakov and R. F. Trunin, *Izv. Akad. Nauk SSSR, Ser. Fiz Zemli* **26**, 72 (1990) [*Izv. Acad. Sci. Phys. Solid Earth* **26**, 952 (1990)].
- [64] R. F. Probststein, in *Theory and Fundamental Research in Heat Transfer*, edited by J. A. Clark (Pergamon, London, 1963), pp. 33–60.
- [65] J. F. Heyda, NASA Report No. NASA CR-1140, 1968.
- [66] A. D. Resnyansky, N. K. Bourne, and J. C. F. Millett, *AIP Conf. Proc.* **620**, 717 (2002); D. J. Chapman, K. Tsembeles, and W. G. Proud, *ibid.* **845**, 1445 (2006).